CHARACTERIZATION OF THE MID-INFRARED WAVELENGTH DEPENDENT LOSS IN HOLLOW CORE PHOTONIC CRYSTAL FIBERS

by

MARY HARNER

B.S., St. Bonaventure University, 2012

A THESIS

submitted in partial fulfillment of the requirements for the degree

MASTER OF SCIENCE

Department of Physics
College of Arts and Sciences

KANSAS STATE UNIVERSITY
Manhattan, Kansas

2015

Approved by:

Major Professor
Brian Washburn

Abstract

This research sought to characterize the length dependent loss of hollow core photonic crystal fibers (HC-PCF) in the mid-infrared. These fibers are used in gas-filled fiber lasers that operate in the mid-infrared range. A black body source which provided a broad mid-infrared spectrum was coupled into a HC-PCF and a fiber cut-back method was implemented to make the length dependent loss measurement. A monochromator was used to observe narrow bands of the broad spectrum provided by the black body source and the loss as a function of wavelength was constructed. The loss for four unique HC-PCF fibers was characterized across the wavelength range λ=1754 nm to λ =3220 nm. The best fibers demonstrated a loss of less than 2 dB/m across this range, with some fibers even exhibiting loss below 1 dB/m.

Table of Contents

List of Figures

List of Equations

Acknowledgements

This work was supported by AFOSR (contract No. FA9950-10-1-00515).

I would like to thank Dr. Fetah Benabid and Benoit Debord for providing the fiber used in this experiment and useful insight into testing the fibers.

I would like to thank Dr. Wolfgang Rudolph and Dr. Vasudevan Nampoothiri for providing useful feedback which helped guide the design of the experimental set-up.

I would like to thank my advisor Dr. Brian Washburn who provided amazing support and guidance throughout my graduate school experience. I would also like to thank Dr. Kristan Corwin for the wonderful help and advice.

I would finally like to thank my friends and fellow graduate students who provided great academic and moral support throughout this experience. Especially, Dr. Rajesh , Dr. Chenchen Wang, Dr. Shun Wu, Neda Dadashzadeh, Turghun Matniyaz, and Kushan Weerasinghe.

Dedication

This is dedicated to my family and loved ones who have loved and supported me through all the crazy: to my mom, Kathy, who has supported me through everything my entire life and my brother, Charlie, and sister, Colleen and their constant reminders to keep things light hearted. Also to my wonderful boyfriend, Paul, who has loved and supported me all along and helped me stay sane. Thanks to all and I love you.

Chapter 1 - Introduction and Motivation

1.1 Introduction

Once of the most obvious and well-known uses of fiber optics is in telecommunications where the objective is ever broadening the transmission bandwidth. Telecommunications typically use a narrow band laser of the near infrared spectrum from 1260 to 1670nm to propagate information through single mode fibers [7]. As technology that utilizes this fiber optics becomes more widespread, a greater demand is placed on the frequencies of light transmitted via optical fibers. The ability to distinguish between bands in the range 1260 to 1670nm is limited. This means that as a greater amount of information is transmitted in the wavelength range easily propagated with existing fiber optics, there are fewer wavelengths available for expanding and including more information. The solution to this problem is twofold, increase the ability to distinguish between smaller and smaller bands of wavelengths, and to increase the range of wavelengths easily transmitted via optical fibers. This experiment is focused on expanding the range of wavelengths useful in fiber optic transmission rather than increasing the ability to distinguish between smaller ranges of wavelengths.

In addition to improving fiber communications, there are also pre-existing lasers that lase in the mid-IR range. It is challenging to incorporate these devices into fiber optic set-ups because the transmission properties of fibers at these wavelengths are either unknown or result in high loss. Some examples of lasers in this range are the Ti: Sapphire and Er-doped lasers [8]. These devices are often used in free space experimental set-ups (*i.e.* the laser is propagated through air and directed using mirrors, lenses and other optical equipment instead of using fibers), but this method is limiting. One major drawback to free-space propagation is the lack of mobility. Slight movement can cause a free-space design to fall out of alignment. This necessitates highly stable tables and little environmental disturbances, such as slamming doors or vibrating walls from pump machines. Another problem with free-space propagation is that it is easily contaminated. Fluctuations in humidity can alter readings from free-space designs due to water absorption. Other contaminant such as dust can be controlled for, but this is cumbersome and an easy source of error. By incorporating fibers in a beam path, wherever possible, less valuable lab space is used and many sources of error are eliminated.

Another area of research that is restricted by a lack of fibers characterized for use in the mid-IR range is gas-filled fiber lasers and fiber references. A gas-filled fiber laser uses a fiber filled with gas as the lasing gain medium [9] [10] [11]. These lasers need fibers that will transmit light at both the pump wavelength and the lasing wavelength. They also need fibers with hollow cores which can be filled with the desired gas. Both of these restrictions make the typically used solid core fibers impractical.

Hollow core photonic bandgap fibers, or HC-PBGF, are useful tools in fiber optics. These fibers utilize photonic bandgap guidance to efficiently guide light over a much broader range of wavelengths than previously achieved [12]. Rather than relying on the total internal reflection of the material's nanostructure, this allows fibers made of cheap and sturdy materials, such as fused silica, to guide wavelengths that it would otherwise absorb. The HC-PBGF use nanostructures to generate region of high and low dielectric constants. These dielectrics are manipulated when fabricating the fibers to allow certain ranges of wavelengths to propagate in the air within the hollow fibers, thus circumventing the absorption of the material [13]. However, these fibers are inefficient at shorter wavelengths. In recent years a new type of hollow core fiber has been developed in response to this limitation, kagome photonic crystal fibers, or kagome HC-PCF. This fiber does not have a photonic bandgap for short wavelength light and the light is allowed to propagate through the cladding [14]. Rather than relying on a photonic bandgap or total internal reflection to guide light, the kagome HC-PCF fibers utilize radial confinement.

The most commonly used fibers are solid core fused silica fibers. These fibers transmit light via total internal reflection. In the visible and shorter near-IR range, these fibers have low loss over long distances [15], and are extremely useful. Unfortunately, any wavelengths longer than the ideal range, typically a wavelength of about 2000 nm [16], are poorly transmitted at best. This happens because much of the light is absorbed by the fused silica glass. The next best options are solid core fibers made of different materials. These different materials have different absorption properties. This changes their total internal reflection and, although they may have low loss in the mid-IR range this may result in high loss in the visible or near-IR range. Different materials have a different window of transmission. A carefully selected material, such as calcium fluoride [17], will have optimum transmission at longer wavelengths in the near-IR and mid-IR range, but will have low transmission in the visible and short near-IR range. Given the restrictive nature of solid core fibers, regardless of material, the next best options are hollow core fibers.

Another advantage to hollow core fibers that cannot be attained using standard solid core fibers is the ability to fill the fiber with gas. Since the light is guided by the fiber through the hollow core, if that core is filled with a gas, the light will also propagate through that gas. This provides many interesting opportunities. One such opportunity is using the gas within a hollow core fiber as a gain medium to produce a laser as long as the pump wavelength and the lasing wavelength both fall within the range of wavelengths guided by fiber [9] [18]. Another application is creating gas filled cells of HC-PCF and splicing them to single mode fibers [11].

There are many varied and useful applications for near- and mid-infrared lasers. Applications range from molecular finger printing [19] and spectral meteorology [20] to defense and communications [21]. Developing lasers that operate in this spectral range is an ongoing challenge hampered by the lack of optics tested for this region of the spectrum. The Lumos/UNFO labs at Kansas State University is in the process of developing optically pumped lasers in this optical range. Andrew Jones, who graduated in 2012, developed a pulsed nanosecond laser that is pumped at 1.5μm using an OPA and lases at 3μm [9]. This laser uses a gas filled fiber as the gain medium. The efficiency of the laser is directly linked with the length of fiber used as the gain medium. The longer the fiber, the higher the gain, but longer fibers also have higher loss [10]. The fibers designed for use in this experiment are untested or poorly tested at the wavelengths of interest for the laser [4]. With knowledge about the fibers' length dependent loss, a more informed choice may be made and the laser may achieve higher gain [9]. Neda Dadashzadeh is continue work on optically pumped fiber gas lasers that could also benefit from knowledge of these fibers' characteristics [9].

This experiment seeks to utilize a reliably constant spectrum from a black body source [22] to characterize the fibers' spectrum from 1754nm through 3220nm. This will allow for more informed decision when choosing a fiber for use in a system with longer wavelengths. The black body source has a known, stable temperature which results in a similarly known emission spectrum. This source was coupled to fibers with unknown characteristics in the longer wavelength range of the mid-infrared range. In order to measure the length dependent loss of these fibers, cut-back measurements were performed by measuring the spectrum transmitted through the fiber, then cutting out a section of the fiber and measuring the spectrum again. This was repeated until the fiber was too short for further cuts. The spectrum was measured by scanning a monochromator across the wavelengths of interest. The voltage was recorded at

regular intervals of approximately 1377nm. Once a full spectrum was recorded, a section of predetermined length was removed. Careful to replace the fiber in the same position and retain the coupling, the measurement was repeated.

To analyze the length dependent loss of the fibers, the spectrum was compared with the length of fiber removed between measurements. This comparison removes concerns about coupling loss [23] and allows accurate characterizations of the fibers despite consistent variations in the source (*i.e.* the shape of the black body spectrum is not flat, so a different power is being provided at different wavelengths, but as long as those different powers are consistent throughout the measurements, they are removed when the power is compared to the length of fiber removed).

1.2 Thesis Outline

The process implemented and the equipment used to perform this experiment will be explored in this paper. Special attention will be given to the reasons for using these specific equipment and procedures. The design of the experimental set-up will be explored in depth and the analysis procedures. The results of the analysis will be presented and discussed.

The general background information, crucial to understanding the operation and design of this experiment, will be explored in the second chapter. The theory surrounding hollow core fibers, black body sources, and monochromators are important to understand the design of this experiment.

The details of the experimental design, equipment used, procedures used to test fiber transmission loss and analysis methods are addressed in chapter three. Many alterations and improvements were made over the course of the experiment to obtain clearer and more useful measurements. Another challenge for this project was reproducibility and will be addressed. The results of the measurements will be explored and discussed in the fourth chapter, including future direction for this project.

Chapter 2 - Background

There are many conceptual ideas that are important to understanding this experiment. These concepts influenced the selection of equipment such as the fibers, light source, and monochromator.

2.1 Fiber Choices

In this experiment kagome hollow core photonic crystal fibers, or kagome HC-PCF, were tested for their length dependent loss in the mid-infrared spectrum. The kagome HC-PCF were provided by our collaborators at Xlim who design and fabricate the fibers, but lack the apparatus necessary to test the transmission in the mid-IR spectrum. These fibers are similar to hollow core bandgap fibers, HC-BGF. They guide light through air in a hollow core utilizing microstructures; however the kagome lattice guides a broader bandwidth than similar fibers which guide light exclusively utilizing the dielectric bandgap created by microstructures. These fibers allow light to propagate in the cladding which provides the opportunity for a much broader transmitted bandwidth. The overlap of the light guided by the core and the cladding provides a promisingly wide band of light propagation [24] [25].

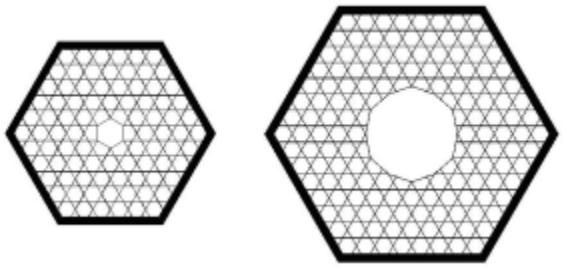

Figure 1 This depicts the fiber end of a kagome hollow core photonic crystal fiber. The image on the left has a core size of one cell and the one on the right has a three ring core. This image was reproduced from Ref. [19].

The fibers used most frequently in fiber optics are solid core fused silica fibers. These fibers are ideal for shorter wavelengths in the visible and near-IR range because they are cheap, durable, and efficient. These fibers use total internal reflection to guide light. The wavelengths a given fiber is capable of guiding is dependent on the material properties of the fiber. Different materials absorb certain wavelengths of light. Also, different pairings of cladding and core affect the angle of total internal reflection for different wavelengths [26]. One solution to the problem of material absorption is to choose a material that has different absorption properties.

Fused silica fibers are most efficient in the visible wavelengths as seen in figure 2. A solid core fiber that transmits well in the near-IR range is Calcium Fluoride or Germanium fibers [27]. These are both options often utilized. There are some drawbacks to these fibers. In order to obtain the higher transmission at the longer wavelengths, the transmission in the shorter wavelengths is sacrificed. Another problem with glasses made of other materials is that they are expensive and extremely fragile. A Zinc Fluoride fiber with a thick protective buffer and jacket is still susceptible to breaking when bent at angles generally acceptable for protected fibers. In addition to sensitivity to bend radius, the glass in these fibers is soft and the ends are easily scratched. Equipment designed to clean fiber ends can scratch Fluoride fiber ends. This is especially problematic as dirty fiber ends will result in poor transmission and fiber loss, but scratched fiber ends from cleaning will also result in loss. Finally, the gas fiber laser that the fibers tested in this experiment will ultimately be used in is incompatible with any solid core fibers. The design of the gas filled fiber laser requires pumping the fiber full of a desired gas and using the fiber as the gain medium for a laser [4]. If the fiber core is filled with material, this experiment will not be possible. In order to address most of these concerns, hollow core photonic band gap fibers, or HC-PBG fibers, are introduced.

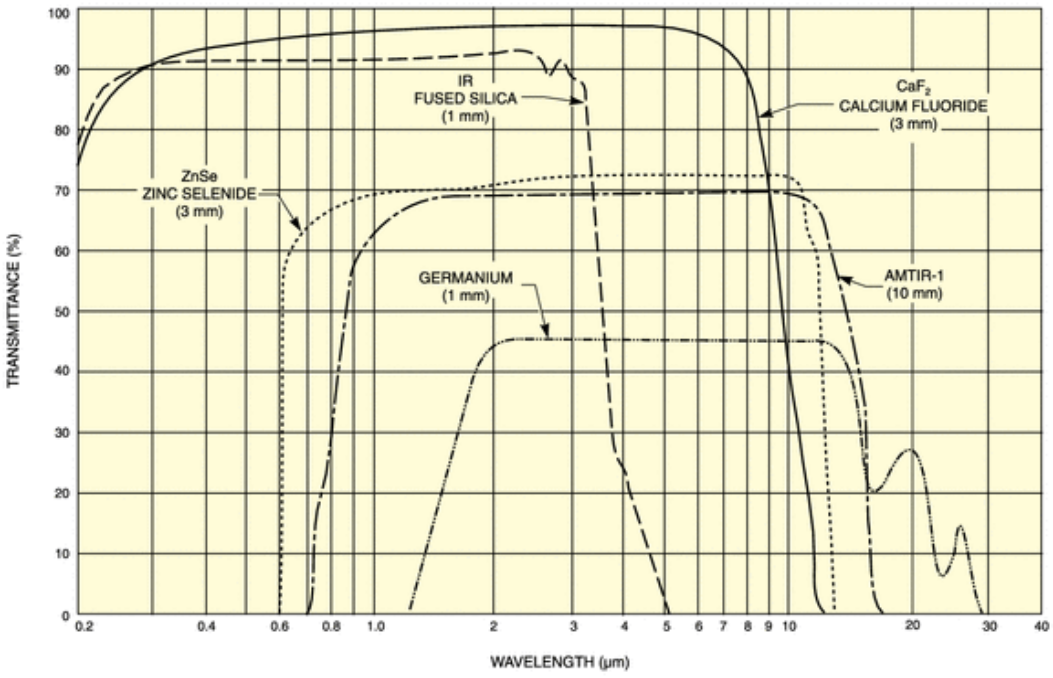

Figure 2 This shows the transmittance of fibers made from various materials offered by Newport. As seen here, the fluoride fiber transmits the largest range of wavelengths in the IR range. This graph was taken from Newport's website [23].

Hollow core photonic band gap fibers use micro structures to act as a waveguide. Rather than depending on the internal reflection of the material to guide the light, these fibers use mismatched dielectrics to guide the light similar to microwaves in metal waveguides [28]. The shape of the microstructure of core along with the shape of the microstructures of the cladding combines to guide the light through photonic bandgap fibers. The cladding is important in these fibers because some modes of light are radiated out of the core and are guided through the cladding. These fibers are useful because they can use any material to guide any wavelength of light. This means the durable materials, such as fused silica, can be used to guide longer wavelengths because the microstructure is guiding the light, not the material. However, the drawback to HC-PBG fibers is that they only guide narrow bands of light [29]. For the gas filled fiber laser, a large range of wavelengths must be guided as the light must be guided at the pump wavelength of 1500nm and the lasing wavelength of 3000nm.

2.2 Black Body Source

A black body source emits a broad spectrum of light based on its operating temperature. Using the following equation one can calculate the spectrum that will be produced by a specific black body source at a particular temperature [2] where $\hbar$ = Plank's Constant, k = Boltzmann's Constant, c = speed of light in meters per second, λ = wavelength range of interest in meters, and T = temperature of black body in kelvin.

$$Power\ Density = \left(\frac{2\pi\hbar c^2}{\lambda^3 \left(e^{\frac{\hbar c}{k\lambda T}} - 1 \right)} \right) \tag{1}$$

Using this equation and the temperature from the manufacturer's statistics, the spectrum for the black body source was calculated as seen in the graph below. To confirm the manufacture's claim an optical spectrum analyzer, OSA, was used to sample a portion of the spectrum. The spectrum produced was limited by the OSA which was designed for viewing light with shorter wavelengths. The small portion of the black body source's spectrum which fell within the OSA's range was recorded then extrapolated to fit the well-known thermal curve of a black body. The spectrum from the OSA was compared the spectrum expected from the device based on the manufacture's information. The similarities between the two spectra were used to confirm the manufacture's claimed temperature.

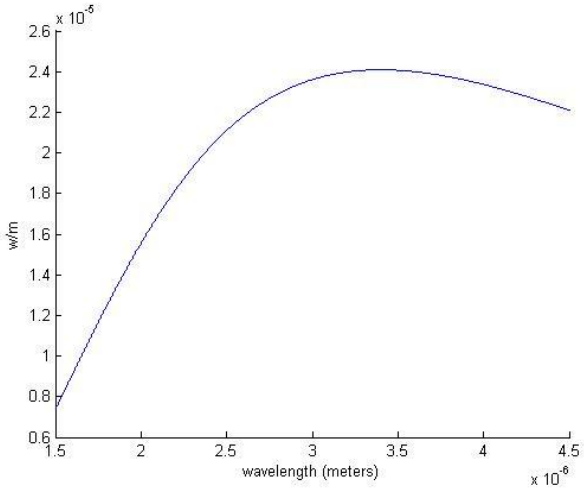

Figure 3 This is the calculated thermal radiation curve for a black body source with a temperature of 1500K.

The most challenging aspect of using a black body for a source rather than a tunable laser is coupling the light into the test fiber. Unlike a laser, a black body source produces incoherent light. This results in a great deal of scattering loss. The light disperses before it can be collimated, much less coupled into the test fiber. The specific model purchased for this experiment, Ocean Optics' Cool Red, was chosen because it is fiber coupled. The device came with a convenient coupling where a patch fiber could be attached to the output.

Previously, a tunable laser was used to test the transmission of fibers. This proved to be an unreliable method. Although the laser could be tuned to the desired wavelengths, slight fluctuations in temperature, both in the tuning process and in the environment, changed the wavelength of the laser [9]. This inconsistency was exacerbated in analysis. When the power transmitted was compared with the length of fiber removed between measurements, an unaccounted for fluctuation in the source intensity introduced error resulting in unreliable results. The black body source was introduced to reduce this error. The black body source doesn't need to be meticulously tuned between wavelengths. By utilizing the broad spectrum produced by a black body, the device was simply turned on and coupled through the test fiber [30]. A monochromator (see section **2.3 Monochromator**) was used to isolate specific wavelengths to accurately characterize the spectrum of the fiber transmission, but the source remained unchanged through this process. This provided a source spectrum that is reliably consistent across each cut back measurement.

2.3 Monochromator

A monochromator is used to separate a broad spectrum into discrete bands. The light enters through a slit which disperses the light to fill a concave mirror. That mirror then focuses the light on a rotating diffraction grating. That grating separates the spectrum of the light and, depending on its angle of rotation, focuses different bands of light on a second mirror. That mirror then focuses the light on an exit slit. The narrowness of the exit slit further selects a specific band of light by blocking other wavelengths. The light that exits the monochromator can then be measured.

All of these components will be essential to adequately test the fibers to a higher standard than they have previously been tested. With the broad spectrum source and monochromator rather than the tunable source previously used, the fibers may be tested with better consistency in measurements and more precise calculations.

Chapter 3 - Set-Up and Procedures

This chapter will explore the specifics of how the experiment was run. The set-up and experimental design will be explained in detail and the procedures will be described in a comprehensive step-by-step manner. This will also cover the evolution of the experiment and some of the hurdles that prompted changes in the initial plan.

3.1 Components

3.1.1 Light Source

The light source used in this experiment is a black body source from Ocean optics named the Cool Red. This source has a temperature of T=1500K providing a spectrum that encompasses the wavelengths of interest for near to mid IR fiber loss measurements [31].

a) b)

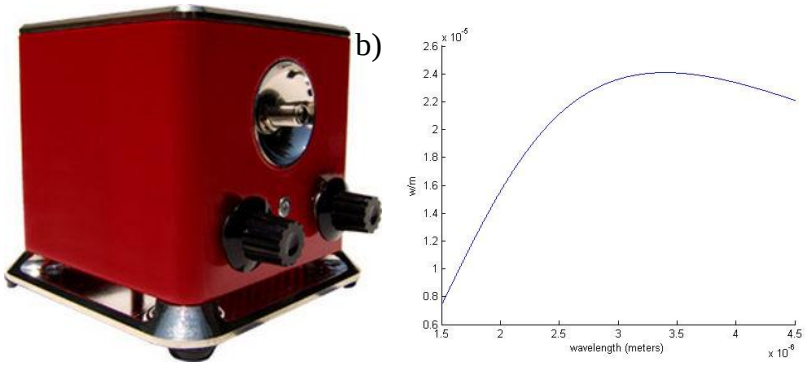

Figure 4 A) is a photo of the black body source from Ocean Optics. The photo was taken from there website [28]. B) is a graph of the thermal radiation curve based on the manufacture's claim that the source's temperature is 1500K.

The light source used in this experiment is a black body source from Ocean optics named the Cool Red. This source has a temperature of T=1500K providing a spectrum that encompasses the wavelengths of interest for near to mid IR fiber loss measurements [31]. The device itself is simple and easy to use. A power cable attaches to the back of the device and there is a DB15 pin connection point in the back of the device as well. This is supposed to connect the Cool Red to a voltage source which can then be used to operate an internal shutter at a programmable frequency, however this feature of the device never worked. An external chopper was used instead. The left most nob was intended for use with the shutter, but because the shutter was never operational the nob was superfluous. The other control on the device was the right most

front panel nob which is the power switch. It can be turned to one of three positions, left most, center, and right most, but left most and right most are both off, while center is on.

The spectrum of the black body source was tested using an optical spectrum analyzer, or OSA. The OSA's range is shorter than that of the black body source, but since the wavelength to power spectrum is well known the data from the OSA was extrapolated to a best fit black body curve as seen in Figure 5 below. This best fit line was then used to confirm the manufacture's claim that the temperature of this device was T=1500K.

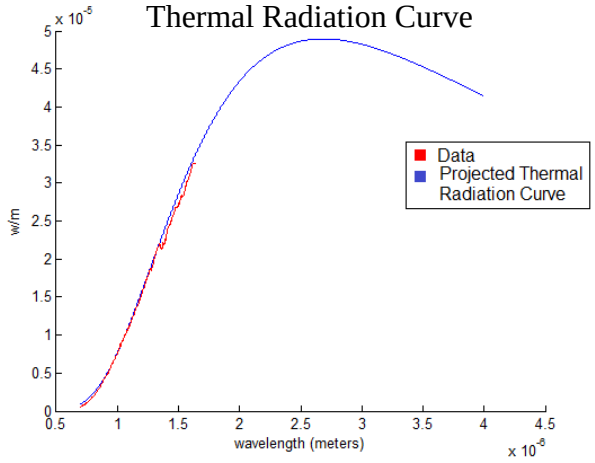

Figure 5 This shows the thermal radiation curve as taken by the OSA in red over the expected thermal radiation curve in blue.

3.1.2 Fibers

There are two types of fiber used in this experiment, a fluoride patch fiber and a hollow core test.

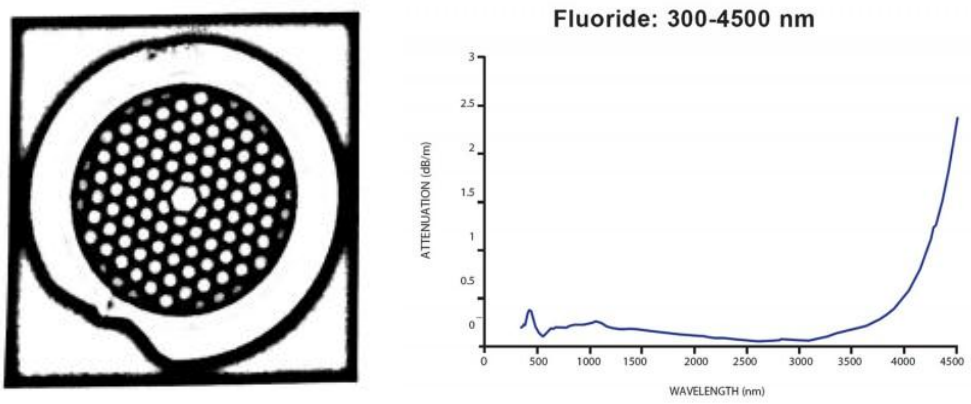

Figure 6 To the left is a photocopy of an image of the end of a single cell kagome fiber taken by a collaborator at Xlim. The image on the right was taken from ocean optic's product description of the fluoride fiber used as a patch fiber in this experiment [30].

The fluoride fiber is a solid core fiber that transmits light via total internal reflection. The material, fluoride glass, transmits light most efficiently in the wavelength range between 500nm and 4000nm. This particular fiber was also chosen because it came with an SMA connector. The specific black body source used in this experiment was designed to accommodate SMA fibers. The fiber ordered from Ocean Optics at the same time as the Cool Red, but when the part arrived it was packaged by Thor Labs. It arrived damaged and, in the future, it will be easier to order directly from Thor Labs as they are an easier company to work with and using Ocean Optics as a middle man resulted in long wait times.

The second fiber is the test fiber that was changed for each measurement. All the fibers tested in this experiment were previously untested kagome HC-PCF fabricated specifically by collaborators at Xlim. These fibers are seven cell three ring kagome fibers. This refers to the size of the core.

3.1.3 Lenses

Half inch Calcium Fluoride plano-convex lenses with a focal length of 2.5cm from Thor Labs were the only lenses used in this experiment. The uncoated CaF lenses were chosen because they were the ideal material to transmit the entire spectrum of the light source. The focal length was chosen based on the numeric aperture of the fluoride fiber, *NA*=0.2. Using the following equation where *D* = 4mm is desired beam waist, *NA* is numeric aperture, and *f* is focal length, it was determined that the ideal focal length would be *f*=10mm. This focal length wasn't available in the desired material. The shortest focal length available was *f*=25mm which produces a beam waist of *D*=10mm. This large beam waist was cumbersome, but it was smaller than all the optics in the beam path. The larger beam waist was deemed workable and the longer focal length lenses were used [3].

$$f = \frac{D}{2NA} \qquad 2)$$

3.1.4 Monochromator

The monochromator used in this experiment is a partially home-built device designed by previous student, Andrew Jones. It includes two concave mirrors, a diffraction grating, and adjustable slits at the entrance and exit.

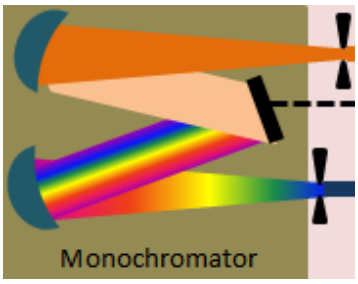

Figure 7 The internal design of a monochromator.

Collimated light entered through the entrance slit which diffused the light. The width of the slit was carefully adjusted until the light filled the first mirror without diffusing beyond the edges of the optic. The mirror reflected the light on a diffraction grating. The rotational angle of the diffraction grating was controlled by a computer using Microsoft Hyperterminal, a terminal emulation program that came with the operating system, Windows XP, which was installed on the computer used. The diffraction grating separated the light into a spectrum. When it was rotated a different portion of the spectrum fell on the second mirror. The second mirror focused that portion of the spectrum on the exit slit. The exit slit blocked all but a narrow band of light from exiting the monochromator. Then an external lens focuses the light on the photodetector.

By controlling the angle of rotation of the diffraction grating, different portions of the spectrum could be viewed with the photodetector. Equation 3 used to align the position of the motor with the wavelengths being shown on the photodetector [4], where p-number refers to a discrete motor positions:

$$\left(\frac{p\ number}{23.87}\right) + 1335 = wavelength\ in\ nm \qquad 3)$$

Where the m-number, here *m*=23.87, represents the how many motor positions or *p numbers* the motor must travel through to scan an entire nanometer of light, and 1335nm is the wavelength where the motor position is zero. The zero position was calculated as part of the calibration process.

To calibrate the monochromator and a laser that produces light at the wavelength 1533 nm was used. The calibrating laser must be at the shorter end of the range accommodated by the monochromator because two fringes must be visible within the monochromator. A laser with a longer wavelength might be visible at the zeroth and first order fringes, but to calibrate the device the first and second order fringes are needed. For a laser of wavelength 1533nm fringes appear at p-numbers p4718 and p41316. To calibrate the monochromator an SMF patch fiber

was used from the laser to the entrance slit of the monochromator. A photodetector capable of detecting the 1533nm light was positioned at the exit slit. Then the monochromator's diffraction grating was scanned across its full range of rotational motion. When a spike in voltage was seen with the photodetector, the monochromator was scanned across that region at smaller and smaller intervals until a peak was found. The *p number* for this peak was recorded and scanning continued until a second peak was found. Using these values, the p number to wavelength ratio can be calculated as follows [4].

$$m = \frac{41316 - 4718}{1533} = 23.87 \quad (4)$$

The monochromator must always be returned to the home position, p0, at the end of a day. If the chip controlling the motor is turned off (*i.e.* if building power goes out), a new home will be set. The position the motor was in when the power was lost will be the new home position or p0 (*e.g.* if the power cuts out while the motor is at position p4718 where the wavelength reflected to the exit slit is 1533, the p0 value will be changed to reflect light of the wavelength 1533 nm on the exit slit and p4718 will reflect the wavelength 1730nm).

In the event that the home is accidentally reset, the first step to fix it is to find out what wavelength is the new home. If the last position of the motor is unknown, the calibration process previously outlined was used with a laser of known wavelength so that the home position can be calculated. Then the monochromator scanned for both fringes. The diffraction grating was stopped at the peak of the first diffraction grating. The following equation was used to calculate the p-number that should correlate with that wavelength. Then, the white wire was disconnected from the control chip on the outside of the monochromator using a small screwdriver. Disconnecting this wire prevented the computer from communicating with the motor while tricking the control chip into thinking it's moving the motor. Hyperterminal was used to turn the grating to the desired p-number. When the hyperterminal program announced the motor was done moving, the white wire was reconnected, completing the process of resting the home position of the monochromator. The calibration of the monochromator was checked again to ensure no unintended alterations were made.

$$(test\ wavelength - desired\ home\ wavelength) \times 23.87 = desired\ p\ number \quad (5)$$

Where the “desired p number” is the position the motor should be in when the wavelength at the undesired home is reflected on the exit slit.

Hyperterminal does not have a command to stop the monochromator mid-movement, so disconnecting the white wire was also used as an emergency stop. The emergency stop was only used in the event that a motor position was accidently entered that could rotate the diffraction grating too far and endangered breaking the grating. The emergency stop compromised the calibration of the monochromator and sacrificed any measurements in progress. Because the monochromator has no organic stop feature, scanning at intervals of p2000 or less is recommended, unless the destination position is known to be much further (*e.g.* when scanning for the second fringe from the 1533nm laser, it would be acceptable to jump from p4718 to p40000 before resuming short scans). The largest p-number presumed safe is p60000 or wavelength 3848nm, however this was never tested.

3.1.5 Lock-In Detector

This device received input from the photodetector (see **3.3.6 Photodetector**) and a chopper positioned in the beam path. The chopper was used as the reference frequency, and the photodetector at the exit slit of the monochromator was connected to input port A. The output of the lock-in detector was attached to an oscilloscope to monitor the fluctuations in voltage readings. The voltage readings had to be taken directly from the lock-in’s display, because there was an unknown scaling factor affecting the signal before it reached the oscilloscope, but the shape of the voltage on the oscilloscope was true to the voltage from the lock-in.

The lock-in detector was set to average the voltage readings over 100s. This long averaging cycle was necessary to reduce noise and provide the best measurements of voltages that were typically on the scale of microvolts.

3.1.6 Photodetector

The photodetector used was a PbSe fixed gain detector designated for use at wavelengths of 1.5-4.8 μm. It was purchased from Thor Labs, product number PDA-20H [32].

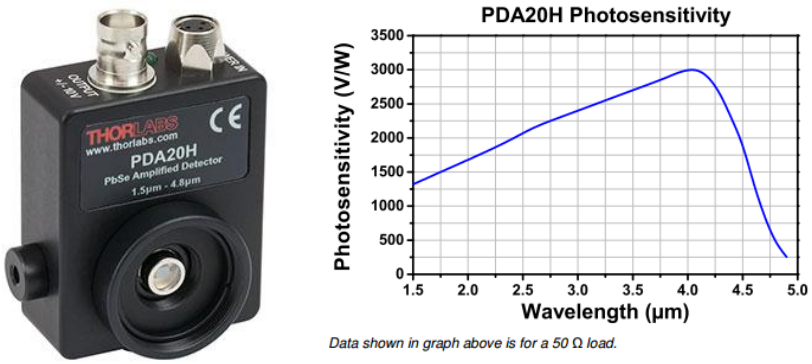

Figure 8 On the left if a photo of the photodetector used in this experiment taken from the product listing on Thor Labs's website. The graph on the right is the photosensitivity of that detector also taken from the product listing on the website [32].

The small detector was easily mounted on an optic post and positioned in front of the monochromator's exit slit using a pair of single axis stages, configured to behave as a two axis stage.

3.1.7 The Set-Up

The final design used is illustrated below in figure 9. The set-up went through many changes over the course of the experiment.

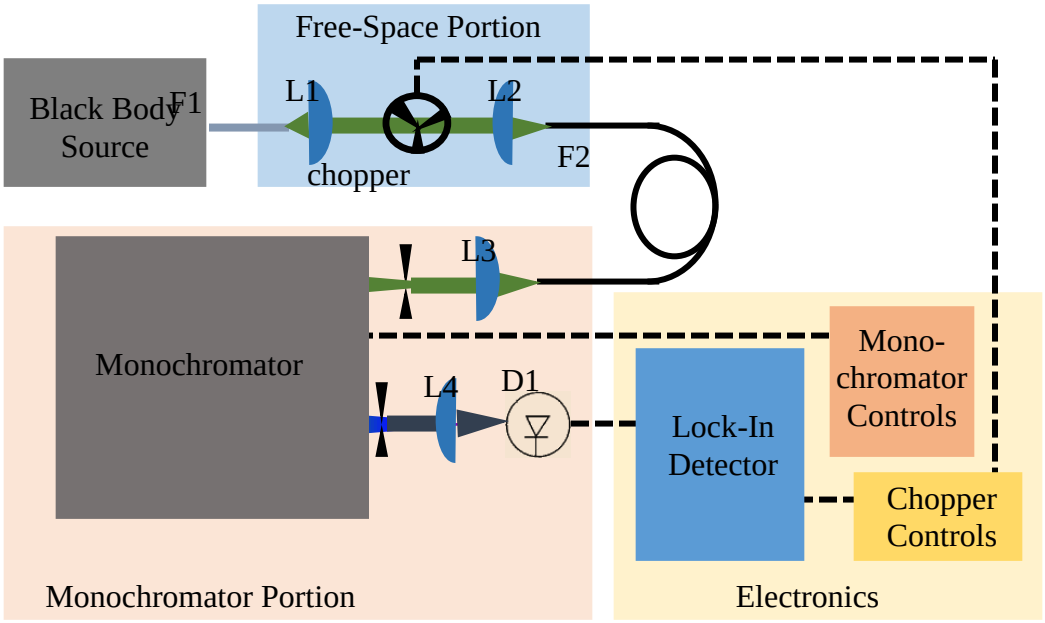

Figure 9 In this diagram. F1 is a fluoride patch fiber and F2 is the interchangeable test fiber. L1, L2, L3, and L4 are all CaF lenses. D1 is a photodetector, specifically ThorLab's PDA 20H. Solid lines are fiber paths and dashed lines are electrical paths.

The set-up that was finally chosen to test the fiber loss of hollow core fiber consists of a black body light source, calcium fluoride lenses, a monochromator, a photodetector, a fluoride fiber, a chopper and a lock-in-detector. The black body source was fiber coupled to a fluoride fiber [33], which guided the light to a coupling stage. The coupling process will be referred to as the Free-Space Portion. On the coupling stage, the light was collimated with a calcium fluoride lens. This lens was not the choice used. Initially zinc selenide lenses were used at this point in the experiment, but these lenses had large focal lengths. The calcium fluoride lenses had much shorter focal lengths that matched well with the patch fiber's large numeric aperture. A chopper was also incorporated in the Free-Space Portion. This was also a change from the initial design. When the light was coupled through the set-up, the light was too faint after the monochromator to be seen on the photodetector over the noise. The noise was on the order of 10mV and the signal was on the order of 10uV. In order to remedy this, a lock-in detector was added to the system. This detector required a frequency reference to pick out the spectrum of interest from the noise. The chopper was placed in the beam line to chop the light to a set frequency and the chopper was used as a reference for the lock-in detector.

The test fiber was then coupled into the monochromator. A five axis stage and calcium fluoride lens were used to collimate the light before it entered the monochromator. Initially there was no lens before the monochromator. The numeric aperture of the fiber was large and it was hoped it would serve to diffract the light adequately to fill the first mirror of the monochromator, but the numeric aperture was too large and the light dissipated before reaching the diffraction grating. There wasn't enough light being transmitted through the monochromator. The lens was added to collimate the light and slits at the entrance of the monochromator were used to diffract the light. The monochromator was then used to select a small band of the transmitted spectrum. The light selected with the monochromator was then shown on a photodetector. The portion of the beam path from being collimated before entering the monochromator through the photodetector will be referred to as the Monochromator Portion. This photodetector was connected to the lock-in detector and was used to measure the voltage of the selected light. The voltage and wavelength were recorded and then the diffraction grating was rotated to select another portion of the spectrum.

With this set-up, the signal from the source was still difficult to identify due to noise. To further reduce this problem a less noisy frequency was selected for the chopper. Initially, the

chopper was operating at 160Hz. To determine the ideal frequency for the chopper, an easily observable wavelength (λ=2466nm) was selected and used for all measurements, then the chopper frequency was varied and the voltage was recorded along with the error bars at each voltage. The size of the error bars represented the noise at each frequency. The noise was plotted against frequency and the least noisy frequency, 670Hz, was used for all subsequent tests.

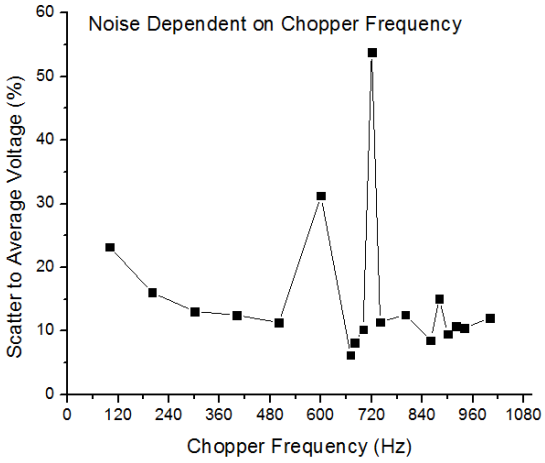

Figure 10 This shows the noise depended loss by chopper frequency. This was used to select the ideal chopper frequency for the experiment.

Once as much noise as possible was removed from the system, there was still a large valley in the spectrum. This valley was at the wavelength λ=2717nm. It was believed that this valley was due to water absorption in the monochromator. Water absorption is known to occur at wavelength λ=1400nm [34] and since the valley was close to λ=2800nm, a multiple of 1400, it was believed this is water absorption as well. To eliminate this feature, a nitrogen drip was added to the system to purge the monochromator of moister. A nitrogen drip involves feeding a line of nitrogen drip into the monochromator and allowing it to leak into the system slowly. This prevents water from accumulating in the device because it creates a slightly higher pressure in the monochromator. Although this did not eliminate the valley, it did diminish the prominence of the feature.

a) b)

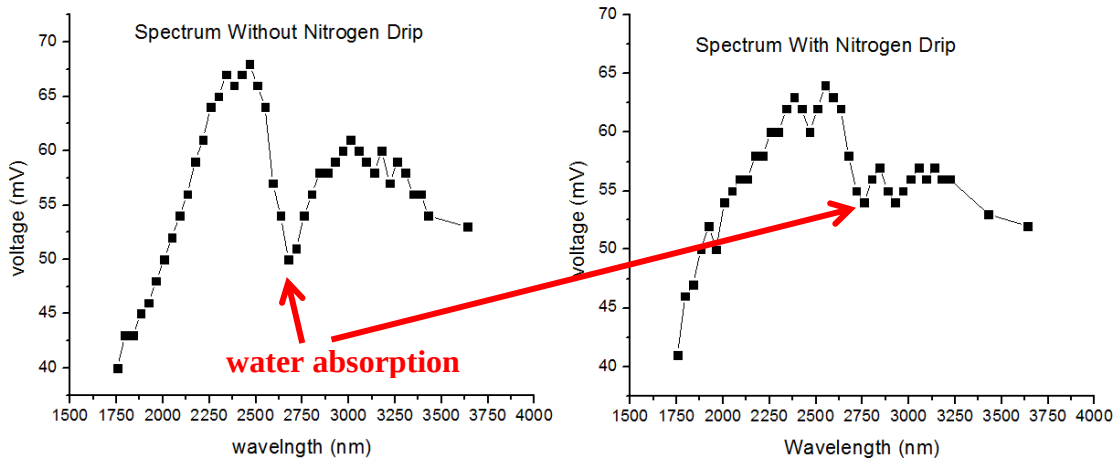

Figure 11 These graphs were used to determine the effectiveness of the nitrogen drip. Graph A was before the drip, and graph B was after.

After the water absorption was eliminated, cutback measurements were made. Through the process of taking cut back measurements, minor alterations were made to restrict fiber movement and further reduce noise, but no more large alterations were made to the experimental design.

3.2 Procedure

To initially align the set-up, a red laser and a laser with a wavelength of λ=1553nm were used. These lasers were used because they were visible (with a spot finding card) through the entire beam line. The red laser was used to make rough, visible adjustments, and the 1553nm laser was used to make finer adjustments. Final alignment adjustments were made using the black body source which was not visible after coupling into the test fiber without use of a lock-in detector.

Once the system was aligned, the monochromator was used in conjunction with the photodetector and lock-in detector to sample the transmission spectrum of the test fiber. The spectrum was sampled over a range from λ≈1754nm to 3220nm. The intervals used were varied depending on the quality of the spectrum from the source and the availability of data in a region from other sources. For shorter wavelengths, collaborators at Xlim have already characterized the fiber's transmission. These wavelengths were measured at a broad interval talking data at wavelengths λ≈1754nm, λ≈1963nm, and λ≈2173nm. Wavelengths longer than λ≈2000nm were untested and received more rigorous attention. Data was taken at regular intervals of λ≈1377nm over the ranges λ≈2173nm - 2592nm. There was interference from water absorption in the monochromator over the interval from λ≈2592nm – 2759nm which resulted in poor

measurements at these wavelengths. Because of this the longer interval of λ≈2754nm was used to take data across this region. At wavelengths longer than the water absorption interference λ≈2759nm - 3220nm the interval was returned to the shorter λ≈1377nm. This results in 26 data points over a range of 1466nm.

Once the desired spectrum was recorded, the fiber end was removed from the entrance slit of the monochromator. A cut back was performed on this end of the fiber, removing segment of the fiber of a predetermined length. The length of the fiber removed was based on the initial length of fiber. The first cut was from the full length of the fiber to approximately 5m. The second cut was between 1.5m to 2m and the final cut was between 1m and 0.5m. The length of fiber removed between spectrum measurements was compared with the spectra. This provided a decibel per meter spectral characterization of the fiber (see **3.4 Analysis Procedure**).

3.4: Reproducibility

A major concern for cut back fiber loss measurements is reproducibility. To make cut back measurements, the fiber must be removed (or partially removed), cleaved, and then be replaced in the exact same position. If the fiber end is not replaced in the exact same place between cuts, there will be a systematic error between cut back measurements that will be obvious when calculating the dB/m loss. If the cleave is not of a consistent quality that will also produce an error. A fiber clamp on a three axis stage was used to hold the fiber on the coupling stage in the Free-Space Portion of the experiment. A similar clamp was used with a five axis stage to align the fiber at the entrance slit in the Monochromator Portion. Once the initial alignment was optimized, the fiber end in the Free-Space Portion was left untouched for the rest of the cut back measurement process. The fiber in the Monochromator Portion was removed and cleaved for each cut back. This was done to prevent misalignment with the source which was the more sensitive coupling stage. The fiber was replaced in the exact same position in front of the entrance slit by measuring the length of fiber that hangs over the edge of the fiber clamp. To maintain a similar cleave between cut back measurements, the same fiber cleaver was used every time. Also, the splicer, which has a fiber viewing camera, was used to view the fiber end and visually ensure a clean cleave.

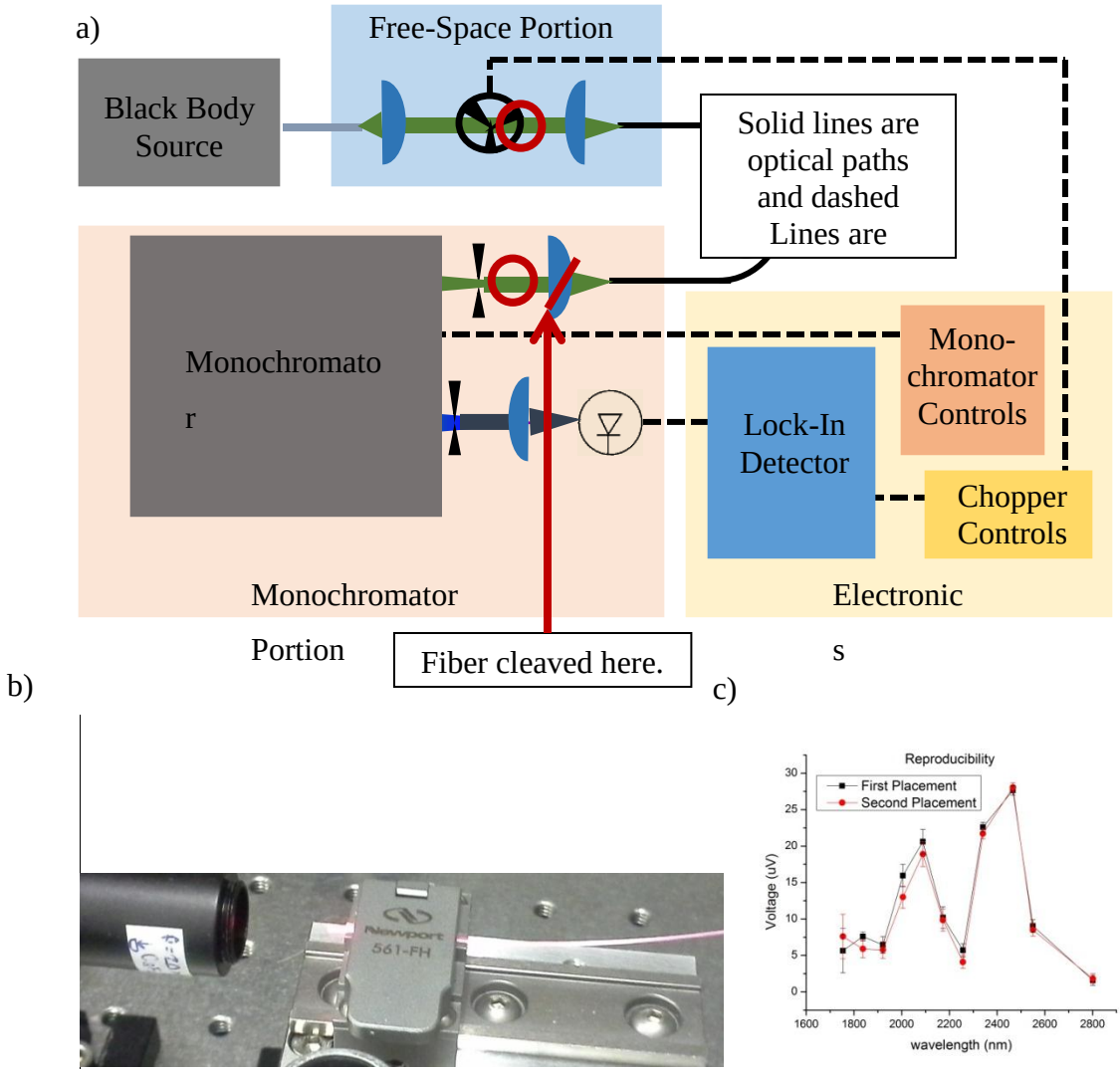

Figure 12 Image A above shows where the fibers were held and cleaved during the cut-back measurements. Image B shows the fiber clamp used and Image C shows the reproducibility.

To test the reproducibility of the fiber replacement method a sparse spectrum of eleven data points was taken while the monochromator sat on a wavelength that was clearly visible through the entire beam path. The sparse spectrum that was used to expedite the process as each data point took approximately five minutes to measure. Once the first spectrum was measured, the fiber end was removed from the fiber clamp at the entrance slit of the monochromator and replaced. The spectrum was then measured again. The graph in figure 12.c above shows the result of this test. This test was applied to both fiber clamps that held the test fiber in the set-up. There was similar reproducibility demonstrated by using this process in the Free-Space Portion and the Monochromator Portion, but performing the cut on the Free-Space Portion end of the test

fiber has the added danger of miss matching modes when replacing the fiber by accidentally rotating the fiber when replacing it. If the fiber was rotated slightly in the coupling stage, the light being coupled into the fiber may not align with the same modes it had aligned with before the cut was made. With this concern in mind, the fiber was consistently cleaved and replaced in the Monochromator Portion where modal mismatch was not a concern since there were no more fiber components past the monochromator and neither the diffraction grating nor the photodetector were mode sensitive.

With this procedure, data was gathered from four different fibers and analyzed. These procedures produce consistent data spectra and reliable fiber loss measurements.

3.5 Analysis Procedure

The most useful loss characteristic for our lab was decibel per meter loss. To find this decibel per meter value, the length of fiber removed was compared with the spectra after each removal. The full length of fiber was first put into the Set-up. Then the spectrum of the light from the source transmitted through the fiber was measured by recording the voltage at twenty six different wavelengths (see **3.4 Procedure**). The fiber was cleaved to five meters. The difference between the full length of the fiber and five meters was recorded. The spectrum was recorded again. The length of the fiber that was removed between these two measurements will be the value used for ΔL when calculating the decibel per meter loss between these two spectrums. Two more meters were removed and another spectrum was recorded. Now, even though only two cut backs have been performed, there are three potential ΔL_1 values and therefore three different decibel per meter loss calculations. The first spectrum and the second spectrum can be compared as described previously. Also the second spectrum and the third can be compared using the two meters as the ΔL_2 value. The third possible decibel per meter loss calculation compares the first spectrum with the third spectrum. To perform this calculation the ΔL value will be calculated by using the sum of the fiber lengths removed between the first and third spectrum so $\Delta L = \Delta L_1 + \Delta L_2$. Over the course of a full loss measurement for a single fiber, three lengths of fiber were removed, leaving four spectra through different fiber lengths. These four spectra provided six possible $\frac{dB}{m}$ values for each data point collected. To calculate the dB/m loss each useful fiber measurement was compared using the following equation [5], where V_s is the voltage measured through the shorter fiber, $V_l$is the voltage transmitted through the longer fiber, and ΔL is the difference in length between the two fibers being compared.

$$\alpha = \frac{dB}{m} loss = \frac{10 \times \log_{10}\left(\frac{V_s}{V_l}\right)}{\Delta L} \quad 6)$$

To find the error in each of these calculations the following equation [6] was derived using error analysis:

$$error = \sqrt{\left(\frac{\partial \alpha}{\partial V_l}\right)^2 {\Delta V_{l\,error}}^2 + \left(\frac{\partial \alpha}{\partial V_s}\right)^2 {\Delta V_{s\,error}}^2 + \left(\frac{\partial \alpha}{\partial \Delta L}\right)^2 {\Delta L_{error}}^2} \quad 7)$$

$$\frac{\partial \alpha}{\partial V_l} = \frac{\partial}{\partial V_l} \frac{10 \times \log_{10}\left(\frac{V_s}{V_l}\right)}{\Delta L} = \frac{10}{\Delta L \times V_l \times \ln(10)}$$

$$\frac{\partial \alpha}{\partial V_s} = \frac{\partial}{\partial V_s} \frac{10 \times \log_{10}\left(\frac{V_s}{V_l}\right)}{\Delta L} = \frac{-10}{\Delta L \times V_s \times \ln(10)}$$

$$\frac{\partial \alpha}{\partial \Delta L} = \frac{\partial}{\partial \Delta L} \frac{10 \times \log_{10}\left(\frac{V_s}{V_l}\right)}{\Delta L} = \frac{-10}{\Delta L^2} \log_{10}\left(\frac{V_l}{V_s}\right)$$

$$error = \sqrt{\left[\frac{10}{\Delta L \times V_l \times \ln(10)}\right]^2 \times {V_{l\,error}}^2 - \left[\frac{10}{\Delta L \times V_s \times \ln(10)}\right]^2 \times {V_{s\,error}}^2 - \left[\frac{10}{\Delta L^2} \log_{10}\left(\frac{V_l}{V_s}\right)\right]^2 \times {\Delta L_{error}}^2} \quad 8)$$

Using this analysis procedure, the dB/m loss was calculated along with error, for each of the twenty six wavelengths measured. These calculations were used to constructed a decibel per meter loss spectrum for four fibers tested.

Chapter 4 - Results and Discussion

This chapter will address the results from the experiment and discuss their implications. Also, the meaning of these results and how they will affect future experiments will be discussed along with future direction for this project.

4.1 Results

4.1.1 Fiber 1

Fiber 1 (120221-CFD-K7C3R-C15J03-fibre-1) received in 2012 has an inner core size of 82µm and an outer core size of 92 µm with a pitch of 22 µm suffered poor reproducibility. This measurement was taken before the decision was made to cleave from the fiber end at the monochromator entrance slit. The large error in these measurements is an example of why the fiber end in the Free-Space Portion should remain untouched. There was also too much loss in the region from λ=2592nm to λ=3011nm for more than one reliable dB/m loss calculation. These challenges prompted more careful cleaving and using the Monochromator Portion end of the test fiber for cut back measurements. Since the different decibel per meter loss calculations were outside error bars for different lengths of fiber removed, this measurement is not useable.

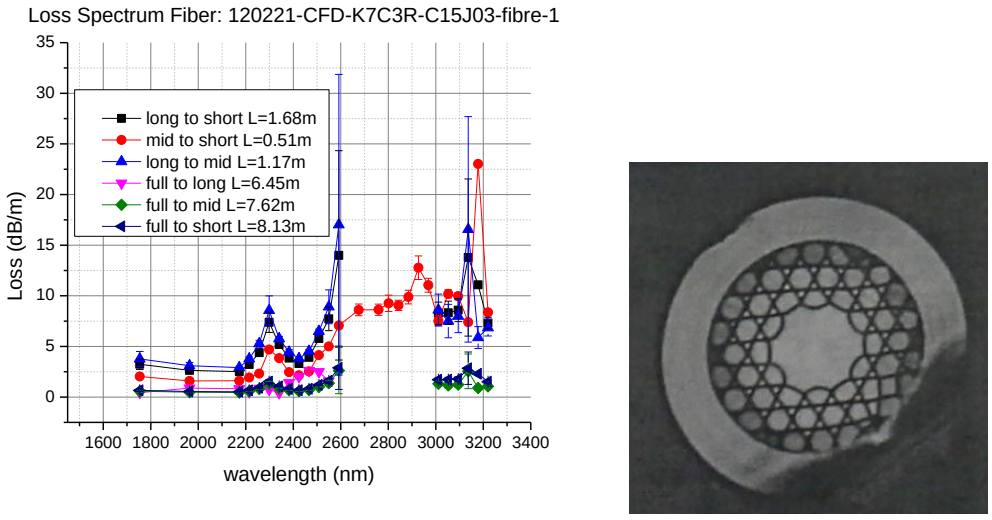

Figure 13 The graph shows the decibel per meter loss of fiber 1. The image on the right is the fiber end of fiber 1.

4.1.2 Fiber 2 and Fiber 3

Fiber 2 (fiber: 120223-CFD-K7C3R-C32J03-fibre-3) was received in 2012 has an inner core size of 84µm and an outer core size of 93 µm with a pitch of 20 µm and fiber 3 (fiber: 12023-CFD-K7C3R-C32J03-fibre-2) was received in 2012 has an inner core size of about 80µm and an outer core size of about 90 µm with a pitch of about 20 µm. The loss measurements from these fibers suffered from a poor cleave on the shortest length of fiber. This was a common problem. The last cut back was limited by the length of fiber needed to stretch from the Free-Space Portion to the Monochromator Portion. A subpar cleave had to be used to ensure the fiber would reach the required distance without placing strain on the fiber during measurements. In this case, the measurements taken with the poor cleave were insufficient and had to be discarded, eliminating three potential loss data sets.

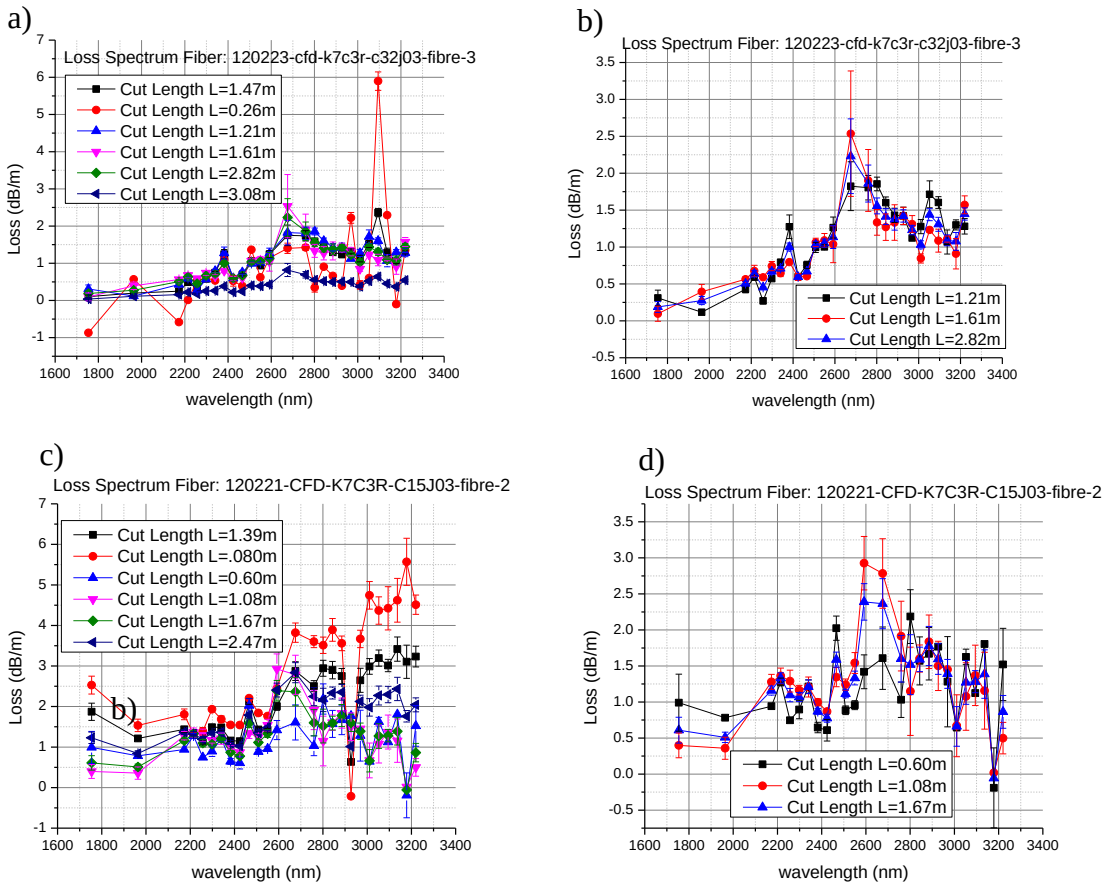

Figure 14 Graph A is the loss of fiber 2 with all data, graph B is fiber 2's loss without poor cleaves. Graph C is fiber 3 with all data, graph D is without poor cleaves.

After elimintating the data from the poor cleave, both of the fibers showed good transmission. Fiber 2 especially, showed less than three decibels of loss per meter across the

spectrum and less than two decibels of loss for light of wavelength 3000nm which is the lasing frequency of the laser these fibers would be most likely used on. Fiber three also showed low loss, but the higher scatter in the data points leaves this fiber as less ideal than fiber 2.

4.1.3 Fiber 4

Before the last loss measurement was taken, the method for securing excess fibers was changed slightly so less tension was placed on the fiber. Fiber 4 (120221-CFD-K7C3R-C15J03-fibre-2) was received in 2012 has an inner core size of about 80μm and an outer core size of about 90 μm with a pitch of about 20 μm and provided the most reliable data and no fiber lengths were discarded. Unfortunately, the monochromator broke halfway through the last measurement. Reparing the monochromator changed the alignment of the entire system and the calibration of the monochromator. This would sacrifice reproducibility beyond redemption. Despite the fact that the shortest fiber length had a clean cleave, the longer wavelengths only have three loss calculations because of equipment malfunction.

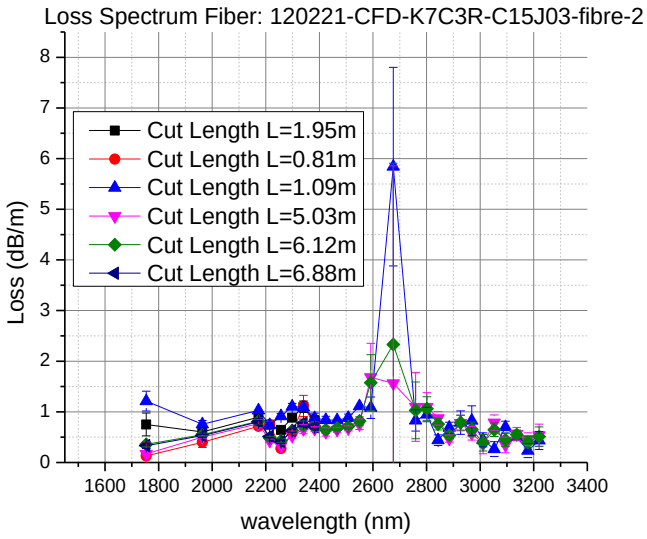

Figure 15 This shows the decibel per meter loss of fiber 4.

This fiber also had the best transmission, excluding one outlying data point, over all had less than two decibels of loss per meter at most wavelengths. At the wavelength of 3000nm or the lasing wavelength of the laser where this fiber will mostlikely be used, the loss was less than one decibel per meter which was better than any of the other fibers tested.

4.2 Discussion

These results will be useful both for use in our lab and in the labs of our collaborators who fabricated the fibers. For the gas filled fiber laser Andrew Jones built, the decibel per meter loss will allow use of a long length of fiber. The longer the fiber, the higher the gain of the laser, until now, the lack of knowledge about the fiber characteristics has forced people using that set-up to use shorter fibers and accept the smaller gain rather than using longer fibers and risking a higher loss due to the fiber that negates the improved gain. Fiber 4 (120221-CFD-K7C3R-C15J03-fibre-2) showed the best transmission across the spectrum and would work well with this laser.

Compared with previous testing methods, this is a marked improvement. Prior to implimentation of this set-up, fiber loss measurements were taken by changing the wavelength of a temperature dependent OPA light source. The meathod for controling the light source was highly subjective to envrionmental changes, especially temperature. Because of the fluctuations in the source, when the spectrums were compared with the length of fiber removed the power readings taken at specific wavelengths were compared with measurements at slightly different wavelengths. The decible per meter loss calculations are highly sensitive to slight fluctuations in power readings, therefore the inconsistency in the source resulted in decible per meter loss measurements with wide margins for error. This experiment has drastic improvment on that margin of error. The following figure shows the fiber loss measuresments as they were prviously taken. Although the fiber is not one that was tested using this meathod, the spread in data points is visible [4].

a)

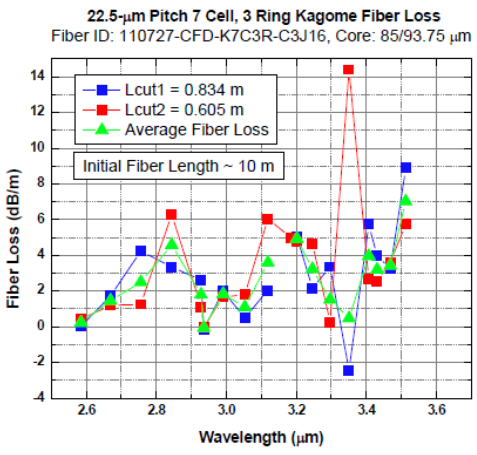

b)

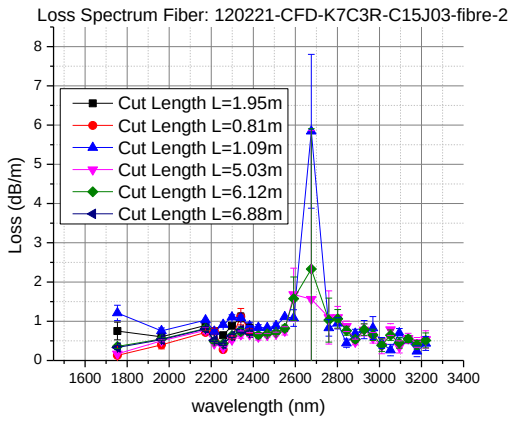

Figure 16 Graph A was taken from Andrew Jones' thesis [16] and shows the decibel per meter loss from a fiber. Graph B shows an example of the decibel per meter loss from this experiment.

Apart from the spread in data points, the old measurements also has a few data points indicating bellow zero fiber loss. This would imply that increasing the length of the fiber would increase the power transmitted which doesn't make physical sense.

4.3 Future Improvement

The immediate next step for these measurements is to test more fibers provided by the same collaborators. This experiment tested all of the seven cell three ring kagome fibers sent to Kansas State University in 2012, but the same year a batch of kagome single cell six ring fibers were sent. Testing of these fibers has already begun. There are other fibers that have been previously tested with less accurate methods. These fibers should be retested using this new method. Then new fibers can be accepted for characterization.

References

[1] S.-J. Im, A. Husakou and J. Herrmann, "Guiding Properties and Dispersion Control of Kagome Lattice Hollow-Core Photonic Crystal Fibers," *Optics Express*, vol. 17, no. 15, 2009.

[2] J. R. Howell, R. Siegel and M. P. Menguc, Thermal Radiation Heat Transfer, CRC Press, 2010.

[3] H. D. Young, R. A. Freedman and A. L. Ford, University Physics with Modern Physics, Addison-Wesley, 2011.

[4] A. M. Jones, "Realizing a Mid-Infrared Optically Pumped Molecular Gas Laser Inside Hollow-Core Photonic Crystal Fiber," Kansas State University, Manhattan, 2012.

[5] Cisco, "Introduction to Optical Fibers, dB, Attenuation and Measurements," 20 April 2005. [Online]. Available: http://www.cisco.com/c/en/us/support/docs/optical/synchronous-digital-hierarchy-sdh/29000-db-29000.html. [Accessed 22 September 2014].

[6] R. R. Haar, "DATA and ERROR ANALYSIS," April 2001. [Online]. Available: http://www.physics.arizona.edu/physics/gdresources/documents/Appendix_%202_Data_analysis.pdf. [Accessed 22 September 2014].

[7] J. Hayes, "Guide to Fiber Optics & Premises Cabling," 2001. [Online]. Available: http://www.thefoa.org/tech/wavelength.htm. [Accessed October 2014].

[8] P. S. Light, F. Couny, Y. Y. Wang, N. V. Wheeler, P. J. Roberst and F. Benabid, "Double Photonic bandgap hollow-core photonic crystal fiber," *Optics Express,* vol. 17, no. 18, pp. 16238-16243, 31 August 2009.

[9] A. Jones, "Mid-infrared gas filled photonic crystal fiber laser based on population inversion," *Optics Express,* vol. 19, no. 3, pp. 2309-2316, 2011.

[10 F. Benabid, G. Bouwmans, J. C. Knight, P. S. J. Russell and F. Couny, "Ultrahigh Efficiency Laser Wavelength Conversion in a Gas-Filled Hollow Core Photonic Crystal Fiber by Pure Stimulated Rotational Raman Scattering in Molecular Hydrogen," vol. 93, no. 12, 2004.

[11 F. Benabid, F. Couny, J. C. Knight, T. A. Birks and P. S. J. Russell, "Compact, stable and efficient all-fibre gas cells using hollow-core photonic crystal fibres," *Letters to Nature,* vol. 434, pp. 488-491, 6 January 2005.

[12 J. Broeng, S. E. Barkou and A. O. Bjarklev, "Photonic Band Gap Fiber". USA Patent US 6845204 B1, 18 January 2005.

[13 R. Cregan, B. J. Mangan, J. C. Knight, T. A. Birks, P. S. Russell, P. Roberts and D. Allan, "Single-Mode Photonic Band Gap Guidance of Light in Air," *Science*, vol. 285, no. 5433, pp. 1537-1539, 3 September 1999.

[14 G. J. Pearce, G. S. Wiederhecker, C. G. Poulton, S. Burger and P. S. J. Russell, "Models for Guidance in Kagome-Structured Hollow-Core Photonic Crystal Fibres," vol. 15, no. 20, 2007.

[15 N. N. S. Karasawa, N. Nakagawa, M. Shibata, R. Morita, H. Shigekawa and M. Yamashita, "Comparison between theory and experiment of nonlinear propagation for a-few-cycle and ultrabroadband optical pulses in a fused-silica fiber," vol. 37, no. 3, 2002.

[16 ThorLabs, "Single Mode Fibers," ThorLabs, [Online]. Available: http://www.thorlabs.com/newgrouppage9.cfm?objectgroup_id=949&pn=SM2000. [Accessed 18 2 2015].

[17 I. D. Aggarwal and G. Lu, Fluoride Glass Fiber Optics, Academic Press, 2013.

[18 V. A. Nampoothiri, W. Rudolph, B. Debord, M. M. Alharbi, F. Gerome and F. Benabid, "CW Hollow Core Optically Pumped Fiber Gas Laser," San Jose, 2014.

[19 S. A. Diddams, L. Hollberg and V. Mbele, "Molecular Fingerprinting with the Resolved Modes of a Femtosecond Laser Frequency Comb," vol. 445, 2007.

[20 J. J. R. Moulton and C. E. Fink, "Ray-Tracing Approach for Realistic Hyperspectral Forest Canopies," 2002.

[21 N. S. Kapany and F. C. Unterleitner, "Fiber Optics Communications Modules". USA Patent US 4329017 A, 11 May 1982.

[22 P. Murdin, "Black-Body Radiation," 2000.

[23 T. P. Hansen, J. Broeng, C. Jakobsen, G. Vienne, H. R. Simonsen, M. D. Nielson, P. M. W. Skovgaard, J. R. Folkenberg and A. Bjarklev, "Air-Guiding Photonic Bandgap Fibers: Spectral Properties Macrobending Loss and Practical Handling," vol. 22, no.

11, 2004.

[24 S.-J. Im, A. Husakou and J. Herrmann, "Guiding Properties and Dispersion Control of Kagome Lattice Hollow-Core Photonic Crystal Fibers," *Optics Express,* vol. 17, no. 15, 2009.

[25 B. Debord, M. Alharbi, T. Bradley, C. Fourcade-Dutin, Y. Wang, L. Vincetti, F. Gerome and F. Benabid, "Hypocycloid-Shaped Hollow-Core Photonic Crystal fiber Part I: Arc Curvature effect on Confinement Loss," *Optics Express,* vol. 21, no. 23, pp. 28597-28608, 2013.

[26 W. B. Spillman Jr and D. H. McMahon, "Frustrated-Total-Internal-Reflection Multimode Fiber-Optic Hydrophone," vol. 19, no. 1, 1980.

[27 ThorLabs, "MIR Multimode Fluoride Fiber Optic Patch Cables," ThorLabs, [Online]. Available: http://www.thorlabs.com/newgrouppage9.cfm?objectgroup_id=7840. [Accessed 19 2 2015].

[28 J. D. Jackson, Classical Electrodynamics, Third Edition Student Edition ed., Singapore: Wiley, 2013.

[29 P. J. Robers, F. Couny, H. Sabert, B. J. Mangan, D. P. Williams, L. Farr, M. W. Mason, A. Tomlinson, T. A. Birks, J. C. Knight and P. S. J. Russell, "Ultimate Low Loss of Hollow-Core PHotonic Crystal Fibers," vol. 13, no. 1, 2005.

[30 C. Gearhart, "Black-Body Radiation," in *Compendium of Quantum Physics*, Springer Berlin Heidelberg, 2009.

[31 Ocean Optics, "Cool Red Light Source," 2014. [Online]. Available: http://oceanoptics.com/product/cool-red/. [Accessed 22 September 2014].

[32 Thor Labs, "PDA20H PbSe Preamplified Detector User Guide," 2 September 2014. [Online]. Available: http://www.thorlabs.com/thorcat/13100/PDA20H-Manual.pdf. [Accessed 20 10 2014].

[33 Ocean Optics, "Fiber Attenuation," [Online]. Available: http://oceanoptics.com/product-category/fiber-attenuation/. [Accessed 19 2 2015].

[34 M. Chaplin, "Water Absorption Spectrum," 27 August 2014. [Online]. Available:

http://www1.lsbu.ac.uk/water/vibrat.html. [Accessed 22 September 2014].